Journal of Materials Chemistry B

Photoresponsive endosomal escape enhances gene delivery using liposome-polycation-DNA (LPD) nanovector

Journal:	*Journal of Materials Chemistry B*
Manuscript ID	TB-ART-04-2018-000994.R1
Article Type:	Paper
Date Submitted by the Author:	12-Jul-2018
Complete List of Authors:	CHEN, WenJie; a. ARC Centre of Excellence for Nanoscale BioPhotonics (CNBP), Department of Physics and Astronomy deng, wei; Macquarie University, Xu, Xin; Macquarie University Department of Chemistry and Biomolecular Sciences, Molecular Sciences; Macquarie University Vo, Jenny; Macquarie University Department of Chemistry and Biomolecular Sciences Zhao, Xiang; Institute of Environment and Sustainable Development in Agriculture, Chinese Academy of Agricultural Sciences Anwer, Ayad; Macquarie University, Department of Physics and Astronomy Williams, Thomas; Macquarie University Department of Chemistry and Biomolecular Sciences Cui, Haixin; Institute of Environment and Sustainable Development in Agriculture, Chinese Academy of Agricultural Sciences, Goldys, Ewa; Macquarie University,

SCHOLARONE™
Manuscripts

Photoresponsive endosomal escape enhances gene delivery using liposome-polycation-DNA (LPD) nanovector

Wenjie Chen[1], Wei Deng[1, 2], Xin Xu[3], Xiang Zhao[4], Jenny Nhu Vo[3], Ayad G. Anwer[1], Thomas C. Williams[3], Haixin Cui[4], Ewa M. Goldys[1, 2]**

1. ARC Centre of Excellence for Nanoscale BioPhotonics (CNBP); Department of Physics and Astronomy, Macquarie University, Sydney, New South Wales 2109, Australia.

2. The Graduate School of Biomedical Engineering, University of New South Wales, Sydney, New South Wales 2052, Australia

3. Department of Molecular Sciences, Macquarie University, Sydney, New South Wales 2109, Australia.

4. Nanobiotechnology Research Centre; Institute of Environment and Sustainable Development in Agriculture, Chinese Academy of Agricultural Sciences, Beijing 100081, P. R. China.

KEYWORDS: light responsiveness, gene delivery, endolysosomal escape, imaging analysis

Corresponding authors

*Email: W.D. wei.deng@unsw.edu.au. E. G: e.goldys@unsw.edu.au.

ABSTRACT

Lipid-based nanocarriers with stimuli responsiveness have been utilized as controlled release systems for gene/drug delivery applications. In our work, by taking advantage of high complexation capability of polycations and the light triggered property, we designed a novel photoresponsive liposome-polycation-DNA (LPD) platform. This LPD carrier incorporates verteporfin (VP) in lipid bilayers and the complex of polyethylenimine (PEI)/plasmid DNA (pDNA) encoding EGFP (polyplex) in the central cavities of liposomes. The liposomes were formulated with cationic lipids, PEGylated neutral lipids and cholesterol molecules, which improve their stability and cellular uptake in the serum-containing media. We evaluated the nanocomplex stability by monitoring size changes over six days, and the cellular uptake of nanocomplex by imaging the intracellular route. We also demonstrated light triggered the cytoplasmic release of pDNA upon irradiation with a 690 nm LED light source. Furthermore this light triggered mechanism has been studied at subcellular level. The activated release is driven by the generation of reactive oxygen species (ROS) from VP after light illumination. These ROS oxidize and destabilize the liposomal and endolysosomal membranes, leading to the release of pDNA into the cytosol and subsequent gene transfer activities. Light-triggered endolysosomal escape of pDNA at different time points was confirmed by quantitative analysis of colocalization between pDNA and endolysosomes. The increased expression of the reporter EGFP in human colorectal cancer cells was also quantified after light illumination at various time points. The efficiency of this photo-induced gene transfection was demonstrated to be more than double compared to non-irradiated controls. Additionally, we observed reduced cytotoxicity of the LPDs compared with the polyplexes alone. This study have thus shown that light-triggered and

biocompatible LPDs enable improved control of efficient gene delivery which will be beneficial for future gene therapies.

1. INTRODUCTION:

Gene therapies currently under development against cancer, genetic disorders, and other diseases utilize diverse genetic materials including antisense oligodeoxynucleotides (asODN), small interfering RNA (siRNA), plasmids and other forms of nucleic acids[1, 2]. While viral transfection remains the established method of their delivery, recently, various nanoscale nonviral vectors have been identified to deliver these genetic materials into cells with several advantages[3-5]. Many of these are comparatively easy to prepare, and they have attractive properties such as minimal immunogenicity and excellent biocompatibility[6], as well as the ability of loading long DNA fragments.[7-9] Besides, the enhanced permeability and retention (EPR) effect enables these nanoscale carriers to preferentially accumulate in tumour tissue[10], and they can also be molecularly targeted[11, 12]. This EPR effect can markedly reduce side-effects towards non-cancer tissue during therapy. All these advantages point to the possibility of nonviral carriers to play a vital role in the future clinical gene/drug delivery systems[8].

Among nanoscale nonviral gene vectors, cationic phospholipids (lipoplexes), polymers (polyplexes) and lipid-polymer hybrids (lipopolyplexes) have been widely developed for various delivery strategies[13]. Lipoplexes are constructed from phospholipid molecules which generally consist of hydrophobic tails and hydrophilic heads. These molecules reassemble to form liposomal or micellar structures able to encapsulate nucleic acids and prevent them from degradation[14]. In cationic liposomal gene carriers, two main forces contribute to the lipoplex formation. One is the elasticity forces driven by the lipid

hydrophobic moiety, the other is the electrostatic force between the negatively charged nucleic acid cargos and the positively charged groups in lipid molecules[15]. Their relative balance may be correlated with lipoplex morphologies and the effectiveness of transfection[16]. Moreover, the fusogenic mechanism induced by the liposomal structure affects cellular internalization of liposomes within the endocytosis pathway, and may promote endosomal escape via membrane destabilization, resulting in content release from liposomes into the cytoplasm[17, 18]. To achieve the on-demand content release, several types of stimulus-responsive liposomes have been designed whose bilayer would be destabilized by physiological and external stimuli [19-23]. These triggering approaches include changes in pH[20], temperature[21], ROS[22], magnetic fields[24], ultrasound[25] or light[23]. Among these, the light-triggering modality has attracted intense interest, due to precise control of different parameters of light, the feasibility of spatiotemporal manipulation (including optical fibre delivery directly into the body) and non-invasiveness of light irradiation. In addition to the controllability of lipid-like delivery systems, their stability in the physiological environment is also crucial for *in vivo* applications. This can be achieved by either adjustment of lipid components or the modification of liposome surface. For instance, incorporating cholesterol (Chol) in liposomal formulations can improve resistance to liposome aggregation in a physiological environment, protect them from protein binding and mechanical breakage[26] and prolong their half-lives. Additionally further surface modification with polyethylene glycol (PEG) the uptake by the mononuclear phagocyte system and extends their blood-circulation time by forming the “stealth liposomes”[27]. Importantly, PEG groups may facilitate conjugation with different targeting ligands

including folic acid, antibodies, and cell penetration peptides (CCP)[28]. All of these are important in *in vivo* applications[29].

Polycation vectors such as PEI[30] and poly-L-lysine (PLL)[31] have been widely used for the formulation of DNA-polymer complexes (polyplexes) for improved DNA delivery into cells. The delivery of polyplexes into cells is facilitated by their high cationic charge density at physiological pH[32]. Although PEI has good physical stability, is easy to manipulate and is moderately resistant to enzymatic degradation[33], its drawbacks such as high cytotoxicity and limited transfection activity have hindered its applications *in vivo*[8, 34, 35]. They are determined by the physicochemical properties of PEI structures and molecular weight. For example, branched PEI with a high molecular weight (for example, 25 kD) shows substantial transfection activity but suffers from the greater cytotoxicity (80%, at 60 μg/mL in Lovo cells) [36], compared with PEI of lower molecular weight[37-39]. To achieve the optimal balance between cytotoxicity and transfection efficiency, different strategies for PEI modification have been explored, including combining the PEI/DNA complex with various phospholipids to form the LPD complexes (named lipopolyplexes)[40].

The purpose of our work is to further enhance the transfection efficiency of such LPD by using external stimuli, for example, light. To the best of our knowledge, few work on photo-responsive LPD as a gene vector has been studied. To this end, we herein developed PEGylated and light-triggered liposomes incorporating large PEI (branched, 25 kD)/pDNA (4.7 kbp) complexes based on our previous work[41]. This photoresponsive LPD successfully delivered gene and achieved gene expression in HCT116 cell line, which is considered as an typical *in vitro* model to study gene therapy of colorectal cancer[42]. The pDNA loading capability of LPD was assessed by gel electrophoresis under different N/P molar ratios (N

indicates PEI nitrogen and P represents phosphate of pDNA). To enhance the stability of LPDs, in addition to PEGylation, Chol was also added to the liposome formulations. The liposome stability with different Chol contents was measured by dynamic light scattering (DLS) and differential scanning calorimetry (DSC). In order to enable light triggering, we used verteprofin (VP). VP is one of the photosensitizer drugs clinically used for photodynamic therapy. VP can rapidly and effectively generate reactive oxygen species (ROS) under 690 nm photoirradiation[43]. When VP is incorporated in the liposome, the ROS production upon irradiation can destabilise the liposomal membranes[41]. We hypothesize here that, after the liposomes have been endocytosed by cells where they eventually localize in the endosomes or lysosomes, the ROS can further destabilize the endolysosomal membranes, resulting in the escape of entrapped pDNA out of the endolysosomal compartments into the cytoplasm, in which the released pDNA can play the role of gene expression. To demonstrate this process of light activated release of pDNA from the endolysosomes, subcellular tracking of endolysosomal escape of pDNA was carried out by confocal microscopy imaging and quantitative analysis of colocalization. Finally, light-enhanced transfection efficiency was examined using flow cytometry to determine the fraction of transfected, EGFP-expressing cells for different light illumination periods. The details of this approach are shown in Scheme 1.

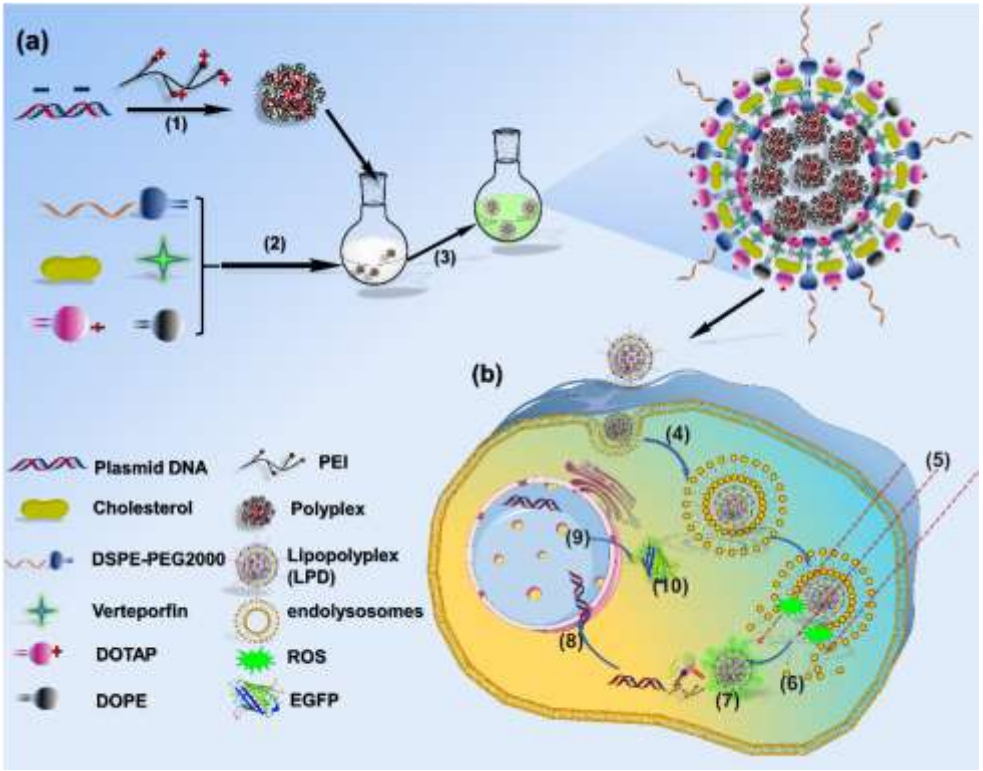

Scheme 1 (a) Schematic illustration of preparation of LPD and (b) intracellular events in the course of light-triggered gene transfer, (1) Polyplex complexation (2) Dried in vacuum (3) Hydration (4) Cellular uptake (5) 690 nm photoirradiation (6) Endolysosomal escape (7) Vector dissociation (8) Nuclear translocation (9) Gene transcription (10) EGFP expression.

2. Experimental

2.1 Materials

Lipids (DOTAP: Catalog No. 890890 and DOPE: Catalog No. 850375, DSPE-PEG (2000) Amine: Catalog No. 880128) were purchased from Avanti Polar Lipids (Alabaster, AL, USA). Dulbecco's modified Eagle's medium (DMEM: Catalog No. 11965-092), fetal bovine serum (FBS: Catalog No. 10437-028), trypsin (Catalog No. 15400054), LysoTracker (Catalog No. L7528), Hoechst 33342 (Catalog No. H3570), Phosphate-

buffered saline (PBS: Catalog No. 10010023) and Dulbecco's Phosphate-buffered saline (DPBS: Catalog No. 14190250) solution, Hank's Balanced Salt Solution (HBSS: Catalog No. 14175145) solution, 4-(2-hydroxyethyl)-1-piperazineethanesulfonic acid (HEPES: Catalog No. 14185052) buffer, TAE Buffer (Tris-acetate-EDTA, 50×, Catalog No. B49) optiMEM (Catalog No. 31985070) solution were purchased from ThermoFisher (Scoresby, Vic, Australia). McCoy's 5A medium (product no: ATCC® 30-2007™), were purchased from the ATCC. Uranyl acetate (Catalog No. 73943), paraformaldehyde (Catalog No. P6148), chloroform (Catalog No. 372978), cholesterol (Catalog No. C8667), Fluoromount™ aqueous mounting medium (Catalog No. F4680), DNase I (Deoxyribonuclease I, Catalog No. D5025), phosphotungstic acid (PTA, Catalog No. P4006) and 2’, 7’-Dichlorofluorescin diacetate (DCF-DA) (Catalog No. D6883) were purchased from Sigma-Aldrich (Castle Hill, NSW, Australia).

2.2 Plasmid DNA and cell lines

The plasmid pEGFP-N1 (GenBank: U 55762.1) encoding the enhanced green fluorescence protein, EGFP (4.7 kbp), was obtained from the Chinese People’s Liberation Army Military Academy of Medical Sciences (Beijing, China). It was amplified in the *E. coli* DH5α strain, extracted and purified using the Qiagen Plasmid Midi Kit. The concentration of the pEGFP-N1 solution was determined with NanoDrop 2000 (ThermoFisher, Vic, Australia). The fluorescein labelled pDNA was prepared using the Label IT® Nucleic Acid Labelling Reagents (Mirus Bio LLC., WI USA) as per the manufacturer’s instructions.

A human colorectal cancer cell line, HCT116 (product no: ATCC® CCL-247™) were purchased from ATCC (Manassas, VA USA). McCoy's 5A medium supplemented with

10% FBS and 1% Antibiotic-Antimycotic was used to culture the HCT 116 cells. DMEM supplemented with 10% FBS and 1% Antibiotic-Antimycotic was used as the culture medium of the HCT 116 cells. The cells were grown at 37 ℃ with 5% CO_2 in the cell incubator. When cells reached about 90% confluence, they were detached with trypsin and transferred into petri dishes or well plates for different experimental purposes.

2.3 Preparation of liposomes and LPDs

Liposomes with different formulations were prepared via a thin-film method[44] with some modifications. Briefly, lipid components at different mole ratios were mixed with VP at the fixed amount in 5 mL chloroform in a round flask (Scheme 1). The mixture solvent was then evaporated under argon gas stream with a rotary evaporator (Buchi R-300, Flawil Switzerland) for 15 min at 50 ℃. The thin lipid film was formed at the bottom of the flask and subsequently hydrated with HEPES buffer (40 mM, pH 7.4) by vigorous stirring for 30 min until the suspension was homogenized. The hydrated liposome suspension was extruded 11 times through a 200 nm polycarbonate membrane in a mini-extruder (Avanti Polar Lipids). The final liposome suspension was purified by using 3000 MW dialysis tubes for 24h at 37 ℃in 500 μL DI water prior to further use. To determine the encapsulation amount of VP loaded inside of liposomes, we added Triton X-100 (0.1%) to as-prepared liposome solution, resulting in VP release. The VP fluorescence (excitation/emission: 425/690 nm) was recorded on a Fluorolog-Tau-3 system and compared with the corresponding VP calibration standard curve. To determine the encapsulation efficiency of VP loaded inside liposomes at different time points (6 h, 12h, 24h, 36h, 48h), dialysis was

conducted. The leaked VP was calculated compared with the corresponding VP standard curve via the fluorophotometer measurement.

The HN buffer (150 nM NaCl and 10 mM HEPES, pH 7.4) is the complexation buffer used for LPD formation. Polyplexes (PEI/pDNA complexes) with different N/P ratios[45] were prepared by incubation of pDNA with different amounts of PEI solution at 37 ℃ in the HN buffer for 30 min. For the preparation of the LPD, the as-prepared lipid film was hydrated with the solution of preformed polyplexes for 30 min at room temperature. The hydrated lipopolyplex solution was freshly prepared prior to cell experiments and measurements.

2.4 Characterization

The zeta potential and size distribution of liposome samples with and without PEGylation were determined by DLS using a Zetasizer 3000HSA (MALVERN Instruments, Worcestershire, UK). After 2 min balance at 25°C, each sample was measured in triplicate and data were collected as the mean ± standard deviation (SD). The size of liposome suspended in different solutions including HEPES buffer, optiMEM medium and 10% FBS solution were also measured at different time points.

Prior to transmission electron microscopy (TEM) imaging of liposome samples, the TEM grid specimens were prepared using the negative staining method. Briefly, a copper grid was placed onto a drop of 10 μL liposome, LPD or polyplex suspension, allowing the grid to absorb samples for 3 min, followed by staining with 2% (w/v) phosphotungstic acid for another 3 min. After air-dry of samples overnight, the grid specimens were then observed under a TEM (Philips CM 10) with an acceleration voltage of 100 KV. Images were captured with the Olympus Megaview G10 camera and processed with iTEM software.

The absorption and fluorescence spectra of liposomes and pure VP were measured with a UV-VIS spectrometer (Cary 5000, Varian Inc.) and a Fluorolog-Tau3 System (HORIBA Scientific) with 425 nm Xe lamp excitation, respectively. To determine the encapsulation efficiency of VP loaded inside liposomes, Triton X-100 (0.1 %) was added to as-prepared liposome solution, resulting in destabilization of liposomal structure and VP release. The VP fluorescence (Ex/Em: 425 nm/690 nm) was recorded on a Fluorolog-Tau-3 system and its concentration was calculated from the standard curve of free VP solution.

For thermal stability measurement, differential scanning calorimetry (DSC2010, TA Instruments, Delaware, US) was used to characterize the temperature of liposome phase transitions (Tm). Briefly, about 10 μL of each sample was placed on an aluminium pan which was covered with an aluminium lid. The pans were heated in a linear gradient (1 °C/min, rising from 25 to 100 °C) in a nitrogen environment, alongside with a reference pan containing 10 μL of HEPES buffer. The peak on each enthalpy graph was indicated with Tm of each sample (data was acquired and exported from the Universal Analysis software).

2.5 Gel electrophoresis

To evaluate the pDNA loading ability of liposomes and determine the best N/P ratio, the electrophoresis using 1% agarose gel (w/v) in TAE (1×) buffer was conducted. The complex solution with various N/P ratios was loaded into the agarose gel. The gel was pre-stained with SYBR Safe DNA stain before running electrophoresis, which was carried for 40 min at a constant voltage of 90 V. Electrophoresis images were then visualized using Gel Imaging U: Genius3 (Syngene, UK). The image acquisition was done using the software GeneSys.

2.6 Enzymatic degradation assay

To assess the capability of LPD for protection of pDNA from DNase I, enzymatic digestion assay was conducted. The LPDs with different N/P ratios were suspended in 1× DNase I Reaction Buffer (10 mM Tris-HCl, 2.5 mM $MgCl_2$, 0.5mM $CaCl_2$, pH 7.6) to a final volume of 50 μl. Two units of DNase I were then added and mixed thoroughly. The mixture solution was incubated at 37°C for 10 minutes, followed by gel electrophoresis analysis described above.

2.7 Cellular uptake of liposomes and endolysosomal escape with light triggering

HCT 116 cells (5×10^4/well) were plated on the coverslips in a 24-well plate and incubated overnight at 37 °C in a humidified 5% CO_2 atmosphere. The cells were then incubated with 500 μL of optiMEM solution containing LPD LPDs (10 μg/mL) for different periods. After incubation, the old media were removed and the cells were washed three times with PBS solution (1 ×, pH 7.4). For the assessment of light-triggered endolysosomal escape of fluorescein labelled pDNA molecules, light irradiation (690 nm, 15 mW/cm^2) using a red LED light source (Fedy, Shenzhen, China,) were carried out for 4 min after 2 hr of incubation of cells with the LPD . For endolysosome staining, LysoTracker (50 nM in optiMEM) was added into the cell culture medium in each well and incubated for one hour before the cells were collected to be fixed. The cells were fixed with 2% paraformaldehyde (10 min, 37℃) and stained with Hoechst 33342 (5 μg/mL) (10 min, 37 ℃). After staining, each coverslip was washed by the PBS solution three times and then mounted onto a glass slide. The glass slide was imaged using a Leica SP2 confocal laser scanning microscopy (CLSM) system. The excitation wavelengths of 405 nm, 488 nm, and 543 nm were used for the confocal imaging of VP, fluorescein labelled pDNA and LysoTracker, respectively.

Their fluorescence emission was imaged at for 460 ± 10 nm Hoechst 33342, 525 ± 25 nm for fluorescein, 590 ± 10 nm for LysoTracker and 700 ± 25 nm for VP.

2.8 Assessment of gene transfection after light illumination

HCT 116 cells were seeded on a 24-well plate at the density of 1×10^5 cells/well, followed by overnight incubation. 500 μL of optiMEM solution containing LPDs (N/P = 25) was added to each well. After 2 h incubation, the cells were exposed to the 690 nm LED light (0.15 mW/cm^2) for 2 min, 4 min, 6 min respectively, followed by additional one hour incubation. The old medium was replaced by the fresh one and the cells were incubated for another 22 h. The EGFP expression in the cells was imaged using a CLSM system. The transfection efficiency of different samples was measured using flow cytometry (CytoFLEX S, Beckman Coulter, Australia). The cells were washed twice and harvested in the DPBS buffer at the concentration of 10^6 cells mL^{-1}, followed by flow cytometry measurements of the percentage of cells expressing EGFP.

2.9 Detection of cellular ROS generation after light illumination

DCF-DA is a non-fluorescent molecule, which can be rapidly oxidized by cellular ROS to the fluorescent DCF. This allows it to be the indicator of a broad range of ROS [46]. In order to quantify ROS generation upon light irradiation, the HCT116 cells (5×10^4/well) were cultured in the petri dishes overnight. After removing the culture medium, the cells were incubated with 500 μL of the optiMEM solution containing LPDs (10 μg/mL). After 2 h incubation at 37 ℃, the medium was removed and the cells were washed with 500 μL of 1× HBSS solution five times. 200 μL of 1×HBSS containing DCF-DA (25 μM) was subsequently added to the cells, followed by incubation for 30 min at 37 °C, while protected from light. After incubation, the cells were illuminated by 690 nm LED light for different

time periods (2 min, 4 min and 6 min). After light irradiation, the DCF-DA solution was removed and cells were washed with PBS three times, followed by imaging under a Leica SP2 CLSM system. For comparison, the control cells were incubated with 100 μL of the optiMEM solution containing H_2O_2 at different concentrations (1 μM, 10 μM and 100 μM) for 2 hours followed by addition of DCF-DA and CLSM imaging. For the determination of ROS, cells were cultivated in 96-well plates, instead of petri dishes, and followed by the same procedure as described above. After treatment, the mean DCF fluorescence intensity in each group was determined by flow cytometry.

2.10 Cell viability assays

The HCT 116 cells were seeded into 96-well plates (1×10^4 per well) and cultured for 24 h at 37°C. The old medium was then removed and the optiMEM solution containing liposomes (10 μg/well, encapsulating VP), lipopolyplex (10 μg/well) and pure PEI (10 μg/well) were added to each well. After 2 hours of incubation, the cells were washed with PBS three times to remove unbound samples. The fresh medium was then added to the cells, followed by another 24 hr incubation. For the light irradiation alone, the cells were exposed to 690 nm light source (15 mW/cm^2) for 1 min, 2 min, 4 min and 6 min, respectively. After light treatment, the fresh medium was added to the cells for another 24 hr incubation. The toxicity of the liposomes, LPDs, pure PEI solution and 690 nm light in cells was assessed using the MTS kit (Promega, WI, USA) as per manufacturer's instructions. Cell viability was calculated as a percentage of the absorbance in treated cells compared with the untreated control cells.

2.11 Statistical analysis

All quantitative data were shown as mean ± SD from at least three parallel groups. *P* values were determined by Student's t-tests or two-way ANOVA (analysis of variance) using Prism 5 (GraphPad). $*p < 0.05$, $**p < 0.01$, $***p < 0.001$ and $****p < 0.0001$ were thought to be statistically significant.

3. RESULTS AND DISCUSSION

3.1 Characterization of pDNA and liposome samples

The morphology and optical properties of pure pDNA molecules, polyplexes and LPD samples were determined by using spectrophotometry and TEM. The plasmid map was plotted using Vector NT and its absorption spectrum is shown (Figure S1a). The absorbance ratios between 260 nm and 280 nm Abs260/Abs280) and between 260 nm and 230 nm (Abs260/Abs230) were calculated to be about 1.8 and 2.0, suggesting high purity of DNA molecules[47]. The TEM images in Fig. 1 show the structure of liposomes loaded with VP (Fig. 1a), pDNA (Fig. 1b), polyplexes (Fig. 1c) and LPDs (Fig. 1d). The PEI/pDNA polyplexes (indicated by red arrows) were observed inside the liposomes as well as on the surface of the liposomes (Fig. 1d). In addition, the VP absorption peak at 690 nm was slightly blue-shifted to a shorter wavelength at 685 nm when loaded inside liposomes compared to VP alone (Fig. 1e), which was consistent with the reported study that liposome's encapsulation causes a blue shift of the loading cargoes[48]. However, the fluorescence spectrum of liposome-formulated VP was not obviously changed compared to pure VP solution (Fig. 1f). These results indicated that VP was encapsulated in the liposomes. The amount of VP loaded inside liposomes was calculated to be approximately 112 μg/mL.

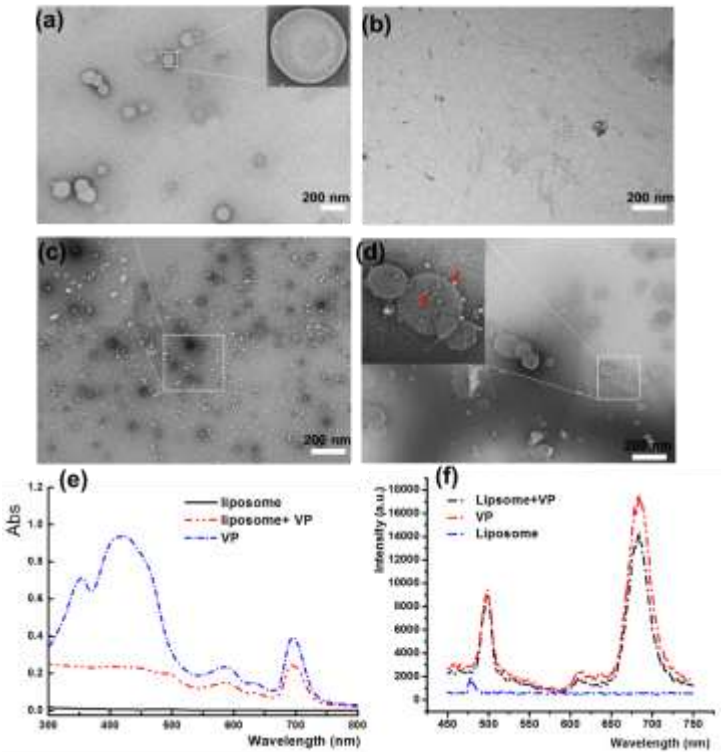

Figure 1 Characterization of different liposome samples. Representative TEM images of (a) liposome loaded with VP, (b) pure pDNA, (c) polyplexes and (d) LPDs. The red arrows indicate the polyplexes. (e) The absorbance and (f) fluorescence spectra of pure liposomes, liposomes loaded with VP and pure VP.

3.2 Stability studies of liposome formulations

Size distribution and zeta potential of liposome formulations with varying Chol content was determined by the DLS method, as shown in Table S1 and Fig S1b. The mean size of liposomes increased with increasing Chol content, up to 150 nm for Chol levels exceeding 50%. These results are consistent with the literature[49]. All the PDI values of nanoparticle suspension are around 0.40, varying slightly between groups with different Chol content. These values indicate a relatively narrow size distribution of the as-prepared LPD[50]. The

zeta potential reduced gradually with the increasing Chol%, because of an increase in the negatively charged hydroxyl group (-OH) on cholesterol.

Chol is a very important component in the liposomal structure which helps to control the rigidity of the lipid bilayer [51]. In order to determine the optimized Chol% for the stabilized liposomes, DLS measurements within six days and DSC assay have been conducted. As shown in Figure S2a and b in the supporting data, the size and corresponding PDI of liposomes with 33% Chol was largely unchanged during 6-day incubation time, compared with other Chol contents; similar results were reported earlier [52]. However, because cholesterol has a very small hydrophilic head and is, therefore, less efficient in shielding the hydrophobic interaction, the excess addition amount of Chol would lead to undesired destabilization of lipid bilayers[53]. Hence, 33% Chol was chosen to formulate liposomes for following experiments.

In addition, the DSC heatflow diagram (Figure. S2c) exhibits the phase transition temperature (Tm) of each liposome with various Chol%. In the absence of Chol, liposomes didn't show any phase change peaks. However, when the Chol fraction reached 50%, the phase transition could be observed. This is because the higher content of cholesterol allows the formation of the anhydrous cholesterol domain in bilayer structure[26], which facilitates the phase transition from solid-gel to a liquid crystal phase. Compared to the liposomes having 50% Chol where the Tm was 55 ℃, the liposomes with a higher proportion of cholesterol (66.7%) exhibited a higher Tm of 72 ℃. The increase in Tm confirms that the addition of cholesterol to the liposome formulation contributes to enhanced stabilization of as-prepared liposomes.

To further demonstrate the stability of PEGylated liposomes in the physiological environment, DLS measurements were conducted to monitor the size changes of PEGylated and non-PEGylated liposomes in the serum-reduced medium (optiMEM) and serum-containing solution (10% FBS cell culture medium). As shown in Figure. S3, the size of conventional liposomes was increased by a factor of two after 6 hr incubation in both the optiMEM medium and normal cell culture medium. However, the PEGylated liposomes liposomes demonstrated a smaller size change did not change so largely compared to non-PEGylated groups ones at the same experimental conditions. In addition, the change of encapsulation efficiency (Figure S3c) of VP with different dialysis time also demonstrated that PEGylated liposomes can lead less leakages of the loaded VP molecules compared to the non-PEGylated groups. These findings indicate that the PEGylation enhances the stability of liposomes during 6 hr incubation compared to the liposomes without PEGylation. The optimal formulation of liposomes with the higher stability is the molar ration of 1:1:1:1 for DOTAP, DSPE-PEG, DOPE and Chol. In addition, VP release profile from liposomes with and without PEGylation also indicated that PEGylated liposomes have higher stability compared to the non-PEGylated ones (Figure 3c).

3.3 The DNA loading capability of LPDs measured by gel electrophoresis

In the presence of polycations or cationic liposomes, the DNA molecules can self-assemble into polyplexes and/or lipoplexes due to electrostatic attraction. An ideal polycation-based gene carrier should have the capability to load a high amount of negatively charged DNA and facilitate cellular uptake. To determine the DNA loading capability of LPD with different N/P ratios used in this study, the agarose gel retardation assays were conducted. The naked DNA molecules without any loading vehicles were clearly observed from the

gel, however, less DNA was detected with an increased N/P ratio (Fig. 2a). When the value of N/P ratio reached 25:1, free DNA could not be detected in the agarose gel lanes, indicating that the maximal amount of DNA molecules can be loaded into the PEI/pDNA polyplexes when N/P ratio reached 25:1.

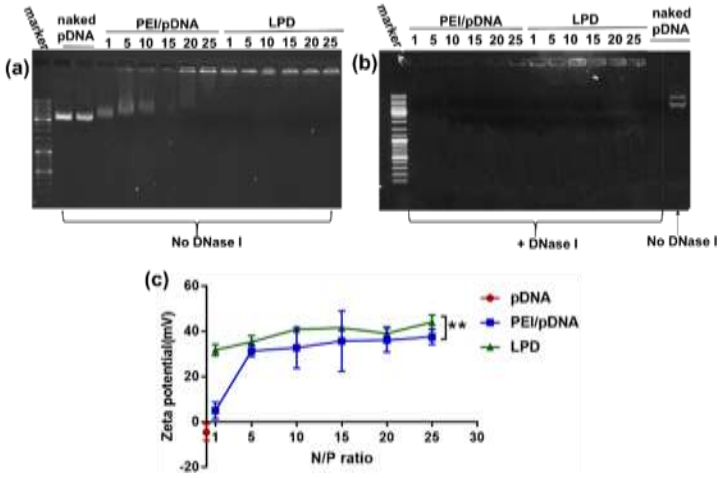

Figure 2 Gel retardation assays of polyplexes and LPDs with different N/P ratios (a) without and (b) with DNase I digestion. (c) Zeta potentials of pDNA, PEI/pDNA, LPD with various N/P ratios. $^{**}p < 0.01$.

It's worth mentioning that LPDs have the higher capacity of condensing negatively charged DNA, compared with the PEI/pDNA polyplex, which was confirmed by the fact that less DNA migrated from the gel wells than the polyplex at same N/P ratio (Fig. 2a,). The condensation of DNA molecules also contributes to the prevention of enzymatic degradation. To demonstrate the reduced enzymatic degradation of DNA in polyplexes and LPDs, the DNase I, a strong endonuclease that non-specifically cleaves DNA, was respectively added into pDNA, polyplex and LPDs for the enzymolysis assay. As shown in Fig. 2b, DNA loaded inside the LPDs at all N/P ratios were clearly visualised in the gel

wells even after the DNase I reaction, while DNA in the polyplex at high N/P ratio only can be observed. For the polyplex at low N/P ratio less than 20 and pure pDNA, there was no clear indication of DNA after enzymatic degradation. These results indicated that the encapsulation of poplyplexes into the liposomal cavity can significantly reduce the enzymolysis effect on cleaving DNA molecules. Therefore, by using this LPD structure, exogenous genetic materials can be protected against undesired enzymatic degradation and delivered to the cells of interest. Additionally, the zeta potential of polyplexes and LPDs with varying N/P ratios was also measured. As shown in Fig. 2c, the zeta potential of different complexes increases with increasing N/P ratio, with higher positive values for LPDs than the polyplex group. This increased positive charge of LPDs would facilitate their cellular uptake through endocytosis pathway due to the preferential interaction between the positively charged delivery platform and negatively charged cell membranes.

3.4 Cellular uptake of LPDs, light-triggered ROS generation, and pDNA release

Fig. S4 in shows representative CLSM images of the internalized LPDs in HCT 116 cells after different periods of incubation (1, 2 and 3 hr). After 3 hr incubation, the perinuclear rings with red fluorescence signal from VP were clearly observed, compared with the cells during 1 hr and 2 hr incubation. Therefore, we chose 3 hr incubation time in this study.

Light-induced cellular ROS generation from LPDs was evaluated by using the DCF-DA assay. In principle, the cell-penetrable nonfluorescent DCF-DA molecules can be oxidized by ROS molecules, resulting in the production of fluorescent DCF. The fluorescence intensity of DCF was increased with light illumination, indicating that a higher amount of ROS was generated from VP loaded inside LPDs than that in non-irradiated cells (Figure. S5). By comparing with the H_2O_2-treated groups which were considered as positive

controls[54], the DCF intensity in the cells treated by LPDs and 6 min illumination was almost equivalent to that produced by 100 μM H_2O_2.

Additionally, cellular pDNA release from LPDs was assessed by irradiating cells with LED light (690 nm, 15 mW/cm^2) for 2 and 4 mins, respectively. As shown in Fig. 3, the increased green signal from the released pDNA (labelled with fluorescein) was clearly observed with light illumination, with the maximum intensity being achieved at 4-min illumination, compared with the absence of illumination. These data indicate that the release of pDNA molecules from the endolysosomal compartments can be enhanced by light irradiation. The reason could be attributed to photochemical damage of endolysosomal membranes caused by increased ROS production due to light exposure.

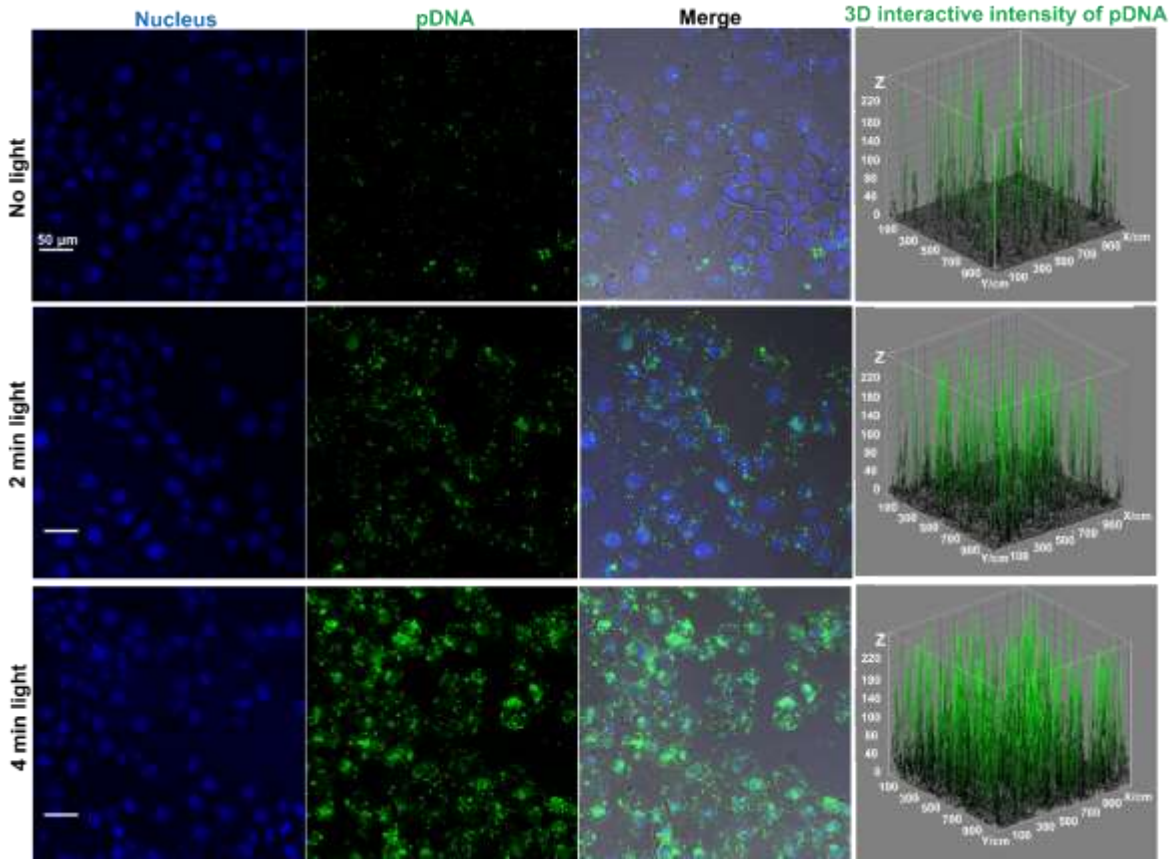

Figure 3 CLSM images and 3D interactive intensity plot of fluorescein-labelled pDNA release after photoirradiation for different periods: 0, 2, and 4 min. The merge panel represent the images merged by the blue, green and bright field channels. Scale bars = 50 μm.

3.5 Quantitative analysis of endolysosomal escape of pDNA after light illumination

To further characterise the enhanced cellular release of pDNA from light-triggered LPDs, intracellular trafficking, and endolysosomal escape were recorded by using CLSM and analysed by the object-based colocalization of fluorescence intensity (Fig. 4), which was done by using the line profile in ImageJ software. After 2 hr incubation, most fluorescein labelled pDNA was observed to be internalized in cells, which was confirmed by the pixel intensity profile (the line profile panel in Fig. 4). These data also show that most of the green signal from fluorescein (pDNA) overlap with the red signal from Lysotracker (endolysosomes) although its intensity is lower than the Lysotracker signal (Fig. 4a). After 3 hr incubation, a stronger overlap between the green and red signal was observed, indicating that the entrapment of LPDs inside the endolysosomes was enhanced after 3 hr incubation, compared to 2 hr (Fig. 4b). However, after a subsequent 4-min light irradiation and another 1 hr incubation, most pDNA molecules escaped outside the endolysosomal compartments. This was confirmed by the reduced overlap between the green and red channels, as shown in Fig. 4c.

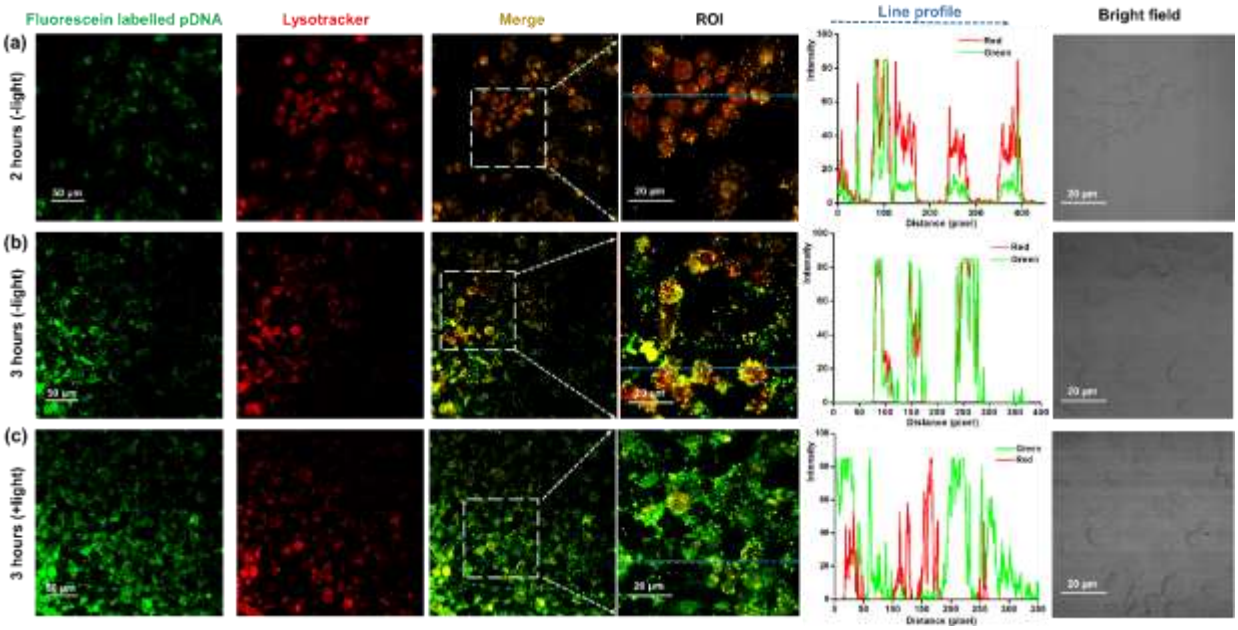

Figure 4 CLSM images of colocalization between the endolysosomes (LysoTracker, red channel) and fluorescein-labelled pDNA (green channel) (a) after 2 hr incubation, (b) after 3 hr incubation and (c) after 3 hr incubation and 4-min light illumination. The line profile plots indicate the intensity distribution of green and red channels through the blue lines in the magnified view of ROI in the merged panel. The right panel presents the bight field pictures of ROI.

To confirm the light-induced escape of pDNA, the colocalization of regions of interest (ROI) shown in Fig. 4 was further quantified using the Costes' approach, Mander's coefficient and the Pearson's coefficient (PC) analysed by using ImageJ. Fig. 5a, b and c show the Costes' maps of the ROIs in Fig 4a, b and c, respectively. Based on the Costes' approach, the colocalization between pDNA and endolysosomes was represented by a white overlay of red signal from LysoTracker and the green signal from fluorescein. A large white area was respectively observed after 2-hr and 3-hr incubation suggesting that most LPD nanoparticles were internalized into the endolysosomes (Fig. 5a and b). However, in

the presence of light illumination, green areas appeared and white areas were significantly reduced, indicating that most LPD nanoparticles were released from endolysosomal compartments into the cytoplasm (Fig. 5c).

Based on the Costes' colocalization analysis, the PC value was also evaluated. The PC ranges from -1 to 1, with -1 indicating a negative correlation, 1 indicating a positive correlation and 0 standing for no correlation. The PC value was 0.859 and 0.801 after 2 h and 3 h incubation without light illumination, respectively, which indicated that most pDNA molecules were colocalized with endolysosomes (Fig. 5d and e). However, the value of PC decreased to 0.633 after light illumination (Fig. 5f), consistent with the pDNA release from the endolysosome compartments.

Furthermore, the Mander's coefficient, varying from 0 to 1, was calculated to determine the overlap fraction of two channels. Here, M1 is defined as the proportion of the green signal coincident with the red signal over its total intensity and M2 is the fraction of green signal coincident with the red one[55]. As shown in Fig. 5g, M2 (indicated by green triangles) was only 44.5% after light illumination, compared with control cells without light illumination (M2 = 99.6%), suggesting that more DNA molecules escaped from endolysosomes after light treatment.

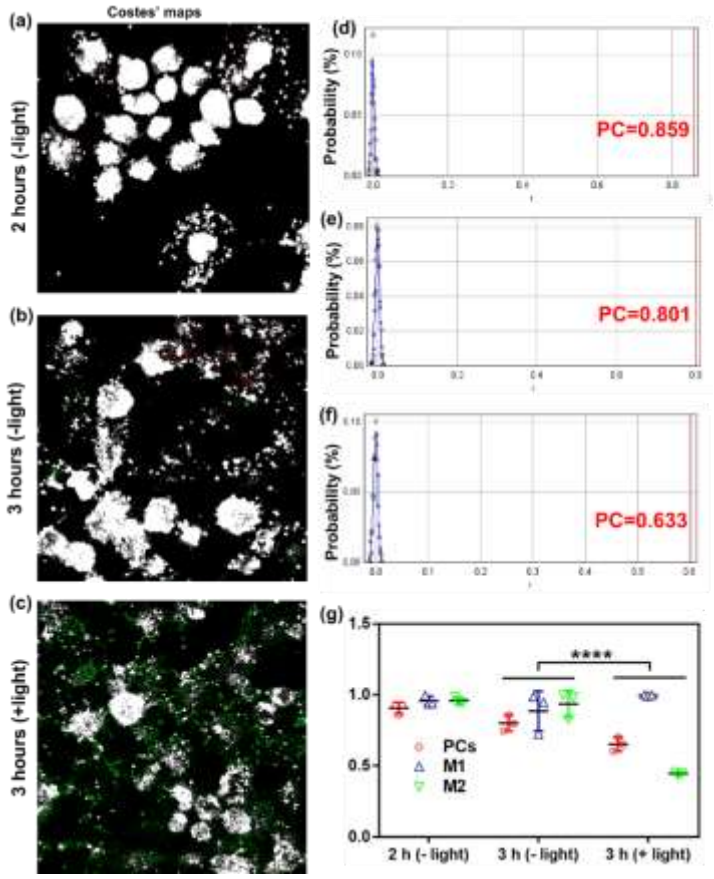

Figure 5 (a), (b) and (c) are the Coste's maps of Fig. 4 (a), (b) and (c), respectively, showing colocalization between pDNA and endolysosomes. (d), (e) and (f) are plots of the distributions of the Pearson's coefficients (PCs) of (a), (b) and (c) respectively. (g) Manders' coefficient analysis and PCs. ****p <0.0001.

3.6 Gene transfection under light irradiation

The CLSM images and quantitative analysis of EGFP expression in HCT 116 cells after light-triggered pDNA release are shown in Fig.6. When cells were treated with LPD (N/P=25) alone, a slightly higher EGFP fluorescence intensity was observed, compared with PEI/DNA (N/P=25) treated cell group (Fig. 6b, c, and h). However, with light illumination, LPD produced enhanced transfection efficiency. The maximum EGFP

expression level was achieved after 4 min illumination (49.3 ± 1.4 %), to a value of over twice that in the LPD transfected cells without light irradiation (20.1± 1.3 %, Fig. 6h). It should be mentioned that, compared with 2 min illumination, the EGFP fluorescence after 4 min illumination shows slightly increasing signal in CLSM images (Fig. 6e and f), but its intensity is changed in a statistically significant fashion (Fig. 6h, $*p < 0.5$). These results are consistent with the pDNA release profile under light irradiation shown in Fig. 3. For comparison purposes, the cells were also transfected with PEI/pDNA polyplexes (N/P=10 and pure pDNA but without light illumination). A lower EGFP fluorescence intensity was observed in these groups, compared with cells transfected by LPDs (Fig. 6a, c, and g), indicating the limited transfection efficiency of PEI/DNA complexes (N/P=10) and pure DNA molecules. Additionally, we evaluated EGFP fluorescence intensity in HCT 116 cells transfected with pure DNA, PEI/DNA complexes and LPDs with and without light illumination by flow cytometry. The representative intensity histograms are shown in Figure S6. The fluorescence intensity of the LPD-transfected groups was increased with prolonged photoirradiation, which confirmed the enhanced transgene efficiency of LPD by photoirradiation.

The maximum transfection efficiency achieved in this study is comparable with previously published work where the combination of branched PEI (BPEI)/pDNA with reduced graphene oxide (rGO) was used to release pDNA under light illumination [56]. In this earlier work, the transfection efficiency of the PEG–BPEI–rGO/pDNA (N/P=20) nanocomplexes in PC-3 and NIH/3T3 cells (with 20-min irradiation at a wavelength of 808 nm, at a light irradiance of 6 W/cm^2) was 2-3 times compared with nanocomplexes alone. However, the involvement of graphene-based materials in this earlier study requires a detailed evaluation

of the toxicity of these materials prior to clinical translation. By contrast, the liposome delivery system used in our work has a high potential for clinical translation due to the long and successful history of using liposomes for encapsulating agents such as Doxorubicin for clinical use.

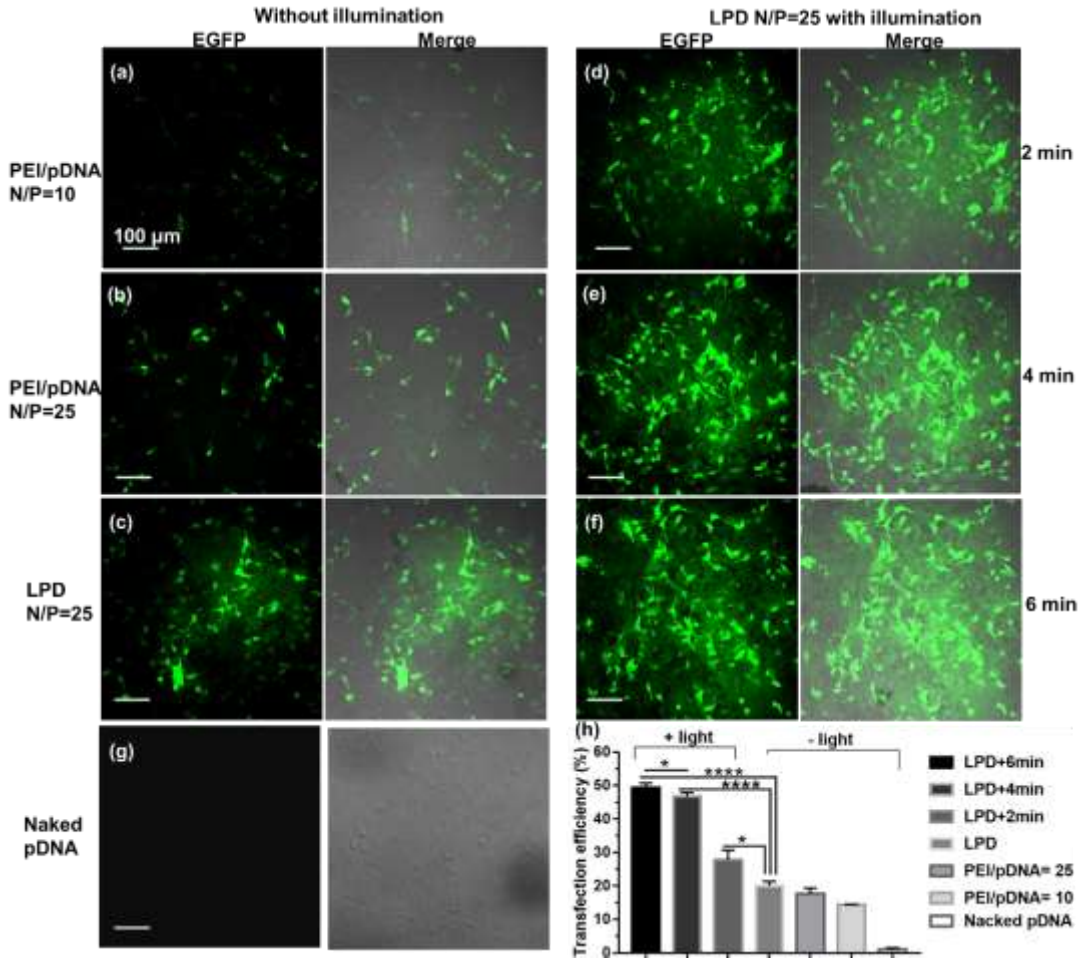

Figure 6 CLSM images (a-f) of EGFP expression in HCT 116 cells after 48 hr of transfection with and without light illumination. Scale bars = 100 μm. (h) transfection efficiencies of different groups. *p <0.05 and ****p <0.0001, compared to the LPD group without light.

3.7 Cellular cytotoxicity assays of different nanocomplexes and light illumination

A series of cell viability tests after the nanocomplex and light treatments were performed to estimate the potential toxicity effect on cells. As shown in Fig. 7, for the light treatment alone, the cell viability was not changed significantly compared to the controls. Among the delivery systems considered in this work, with same concentration at 10 μg/well, PEI has higher toxicity to cells, about 32% cells being affected when treated with PEI and illuminated for 4 min. By contrast, the liposomes and LPDs did not affect cell viability, even under photoirradiation for different time periods. For example, about 17% cells were killed by LPDs after 6-min illumination. This could be a result of the light-triggered ROS generation from VP. However, more than 80% cells were still alive in liposome and LPD groups, indicating that these delivery platforms are relatively biocompatible.

In this study, PEI polyplexes still exhibited their intrinsic cytotoxicity (around 70% cell viability in our experimental conditions). However, the cytotoxicity was significantly reduced by incorporating PEI/pDNA complexes into liposomes. The results on cell viability after treatment with our lipopolyplex and light illumination was even comparable with other liposome-PEI hybrid vectors alone (more than 80% cell viability)[57].

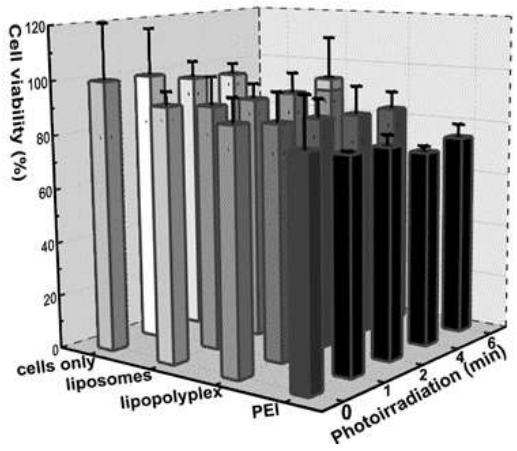

Figure 7 Cytotoxicity of liposomes (10 μg/well), lipopolyplex (10 μg/well) and PEI (10 μg/well) on HCT 116 cells in combination with photoirradiation.

4. CONCLUSION

In summary, a photoresponsive LPD system was developed for pDNA delivery and release *in vitro*. The complexation of DNA and PEI and formation of the LPD nanoconstruct enhanced the loading capacity of pDNA into the liposomal vehicles. Subsequent encapsulation of polyplexes inside liposomes overcame the disadvantages in high cytotoxicity of PEI and photosensitizer molecules. The addition of cholesterol and PEGylated lipids in liposome formulation improved the stability and biocompatibility of nanocomplexes in the physiological environment, which is very important for the use of light-triggered liposomes in *in vivo* applications, in particular, on-demand gene release. The VP molecules introduced into the liposome cavity generated ROS after light illumination, enabling endolysosomal escape of pDNA via a photochemical internalization mechanism. This dynamic process has been demonstrated by quantitatively analysing image-based colocalization between nanocomplexes and endolysosomes. After light triggering, pDNA was released and modified the expression of encoded EGFP in HCT116 cells. The enhancement of EGFP fluorescence intensity by a factor of two was achieved with light-triggered LPD delivery system, compared with the control group without light illumination. In this project, 690 nm LED (15 mW/cm^2) was used as a light source, whose maximum dosage (6 min irradiation) was calculated to be 5.4 J/ cm^2. This is much lower than clinic and *in vivo* dose (25-500 J/ cm^2) of the light source used for activating VP in photodynamic therapy[58, 59]. In addition, the wavelength of 690 nm located within “therapeutic window” can penetrate tissues deeper (5-10 mm) with less photodamage to biological tissues compared with visible light[60]. Given these

excellent properties of this light source, we believe this system can be feasible for *in vivo* work. In addition to pDNA used in this study, our light responsive LPD system can efficiently deliver other nucleic acids including siRNA, microRNA and larger plasmids with specific functions. These genetic materials can be delivered in a temporally controllable way by combining such delivery vehicle with light, thus providing a potential for enhanced transfection efficiency and therapeutic effect in gene therapy *in vivo*. Further clinical translation is also achievable with our liposomal nanocarrier since the key agents including lipids and VP are widely used in clinical practice.

Conflicts of interest

There are no conflicts to declare.

Supporting Information.

Electronic supplementary information (ESI) available. See DOI: XXXXX

ACKNOWLEDGMENT

This work was supported by the Australian Research Council (DECRA: DE130100894 and ARC CoE: CE140100003), the HDR Budget from Macquarie University, the Major National Scientific Research Program of China (2014CB932200) and the National Key Research and Development Program of China (2017YFD0500900). The authors thank Mr. Kai Peng for his assistance of flow cytometry and also thank the Macquarie Microscopy Unit for TEM work.

ABBREVIATIONS

asODN: Antisense oligodeoxynucleotides; BPD-MA: Benzoporphyrin derivative monoacid; BPEI: Branched polyethylenimine; CLSM, Confocal laser scanning microscopy; DDS, Drug/gene delivery systems; DOPE, 1,2-Dioleoyl-sn-glycero-3-phosphoethanolamine; DOTAP, N-[1-(2,3-Dioleoyloxy)propyl]-N,N,N-trimethylammonium methyl-sulfate; EGFP, Enhanced green fluorescent protein; FDA, Food and drug administration; LED, Light-emitting diode; LPEI, Linear polyethylenimine; NIR, Near-infrared; PCI, Photochemical internalization; pDNA, Plasmid DNA; PDT, Photodanymic therapy; PEG, Poly-(ethylene glycol); PEI, Polyethylenimine; PLGA, Poly(D,L-lactide-co-glycolide); PLL, Poly-L-lysine; ROS, Reactive oxygen species; siRNA, Small interference RNA; TEM, Transmission electronic microscopy; VP, Verteporfin; DLS, Dynamic light scattering; DCF, 2’, 7’-dichlorofluorescin; DCF-DA, 2’, 7’-Dichlorofluorescin diacetate; PBS, Phosphate-buffered saline; HEPES, 4-(2-hydroxyethyl)-1-piperazineethanesulfonic acid; TAE, Tris-acetate-EDTA; HBSS, Hank's balanced salt solution; DMEM, Dulbecco’s modified Eagle’s medium; FBS, Fetal bovine serum; DPBS, Dulbecco's Phosphate-buffered saline; DSC, Differential scanning calorimetry; EPR, Enhanced permeability and retention; DMSO, Dimethyl sulfoxide; PTA, Phosphotungstic acid

REFERENCES

1. R. C. Mulligan, *Science*, 1993, **260**, 926-926.
2. R. Srinivas, S. Samanta and A. Chaudhuri, *Chem Soc Rev*, 2009, **38**, 3326-3338.
3. M. S. Shim and Y. J. Kwon, *Adv Drug Deliver Rev*, 2012, **64**, 1046-1059.
4. D.-J. Lee, D. He, E. Kessel, K. Padari, S. Kempter, U. Lächelt, J. O. Rädler, M. Pooga and E. Wagner, *J Control Release*, 2016, **244**, 280-291.
5. D. Luo and W. M. Saltzman, *Nat Biotechnol*, 2000, **18**, 33.
6. H.-X. Wang, M. Li, C. M. Lee, S. Chakraborty, H.-W. Kim, G. Bao and K. W. Leong, *Chem Rev*, 2017, **117**, 9874-9906.
7. S.-d. Li and L.-y. Huang, *Gene Ther*, 2000, **7**, 31.
8. H. Yin, R. L. Kanasty, A. A. Eltoukhy, A. J. Vegas, J. R. Dorkin and D. G. Anderson, *Nature reviews. Genetics*, 2014, **15**, 541.

9. J. A. Kretzmann, D. Ho, C. W. Evans, J. H. Plani-Lam, B. Garcia-Bloj, A. E. Mohamed, M. L. O'Mara, E. Ford, D. E. Tan and R. Lister, *Chemical Science*, 2017, **8**, 2923-2930.
10. Z. Zhou, X. Liu, D. Zhu, Y. Wang, Z. Zhang, X. Zhou, N. Qiu, X. Chen and Y. Shen, *Adv Drug Deliver Rev*, 2017.
11. L. S. Mendonça, F. Firmino, J. N. Moreira, M. C. Pedroso de Lima and S. Simões, *Bioconjugate Chem*, 2009, **21**, 157-168.
12. J. Yang, A. Bahreman, G. Daudey, J. Bussmann, R. C. Olsthoorn and A. Kros, *ACS central science*, 2016, **2**, 621-630.
13. A. Ewe, A. Schaper, S. Barnert, R. Schubert, A. Temme, U. Bakowsky and A. Aigner, *Acta biomaterialia*, 2014, **10**, 2663-2673.
14. R. N. Majzoub, K. K. Ewert, E. L. Jacovetty, B. Carragher, C. S. Potter, Y. Li and C. R. Safinya, *Langmuir*, 2015, **31**, 7073-7083.
15. V. Fehring, U. Schaeper, K. Ahrens, A. Santel, O. Keil, M. Eisermann, K. Giese and J. Kaufmann, *Mol Ther*, 2014, **22**, 811-820.
16. B. Ma, S. Zhang, H. Jiang, B. Zhao and H. Lv, *J Control Release*, 2007, **123**, 184-194.
17. H. Deng, K. Song, X. Zhao, Y. Li, F. Wang, J. Zhang, A. Dong and Z. Qin, *ACS Applied Materials & Interfaces*, 2017, **9**, 9315-9326.
18. L. Yin, H. Tang, K. H. Kim, N. Zheng, Z. Song, N. P. Gabrielson, H. Lu and J. Cheng, *Angewandte Chemie International Edition*, 2013, **52**, 9182-9186.
19. J. Liu, C. Detrembleur, S. Mornet, C. Jérôme and E. Duguet, *J. Mater. Chem. B.*, 2015, **3**, 6117-6147.
20. L. Jiang, L. Li, X. He, Q. Yi, B. He, J. Cao, W. Pan and Z. Gu, *Biomaterials*, 2015, **52**, 126-139.
21. K. Kono, M. Takashima, E. Yuba, A. Harada, Y. Hiramatsu, H. Kitagawa, T. Otani, K. Maruyama and S. Aoshima, *J Control Release*, 2015, **216**, 69-77.
22. X. Liu, J. Xiang, D. Zhu, L. Jiang, Z. Zhou, J. Tang, X. Liu, Y. Huang and Y. Shen, *Adv Mater*, 2016, **28**, 1743-1752.
23. K. A. Carter, S. Shao, M. I. Hoopes, D. Luo, B. Ahsan, V. M. Grigoryants, W. Song, H. Huang, G. Zhang and R. K. Pandey, *Nature communications*, 2014, **5**.
24. R. Di Corato, G. Béalle, J. Kolosnjaj-Tabi, A. Espinosa, O. Clement, A. K. Silva, C. Menager and C. Wilhelm, *ACS nano*, 2015, **9**, 2904-2916.
25. Y. Li, H. An, X. Wang, P. Wang, F. Qu, Y. Jiao, K. Zhang and Q. Liu, *Nano Research*, 2018, **11**, 1038-1056.
26. S.-y. Yang, Y. Zheng, J.-y. Chen, Q.-y. Zhang, D. Zhao, D.-e. Han and X.-j. Chen, *Colloids and Surfaces B: Biointerfaces*, 2013, **101**, 6-13.
27. M. L. Immordino, F. Dosio and L. Cattel, *International journal of nanomedicine*, 2006, **1**, 297.
28. E. Oh, J. B. Delehanty, K. E. Sapsford, K. Susumu, R. Goswami, J. B. Blanco-Canosa, P. E. Dawson, J. Granek, M. Shoff and Q. Zhang, *Acs Nano*, 2011, **5**, 6434-6448.
29. K. Maruyama, T. Yuda, A. Okamoto, S. Kojima, A. Suginaka and M. Iwatsuru, *Biochimica et Biophysica Acta (BBA)-Lipids and Lipid Metabolism*, 1992, **1128**, 44-49.
30. J. Kim, H. Kim and W. J. Kim, *Small*, 2016, **12**, 1184-1192.
31. M. A. Sheikh, Y. S. Malik, Z. Xing, Z. Guo, H. Tian, X. Zhu and X. Chen, *Acta biomaterialia*, 2017, **54**, 58-68.
32. N. W. Kim, M. S. Lee, K. R. Kim, J. E. Lee, K. Lee, J. S. Park, Y. Matsumoto, D.-G. Jo, H. Lee and D. S. Lee, *J Control Release*, 2014, **179**, 11-17.

33. Y. He, Y. Nie, G. Cheng, L. Xie, Y. Shen and Z. Gu, *Adv Mater*, 2014, **26**, 1534-1540.
34. S. P. Strand, S. Lelu, N. K. Reitan, C. de Lange Davies, P. Artursson and K. M. Vårum, *Biomaterials*, 2010, **31**, 975-987.
35. D. V. Schaffer, N. A. Fidelman, N. Dan and D. A. Lauffenburger, *Biotechnol Bioeng*, 2000, **67**, 598-606.
36. Z. Zhan, X. Zhang, J. Huang, Y. Huang, Z. Huang, X. Pan, G. Quan, H. Liu and L. Wang, *Materials*, 2017, **10**, 731.
37. V. Kafil and Y. Omidi, *BioImpacts: BI*, 2011, **1**, 23.
38. M. D. Giron-Gonzalez, R. Salto-Gonzalez, F. J. Lopez-Jaramillo, A. Salinas-Castillo, A. B. Jodar-Reyes, M. Ortega-Muñoz, F. Hernandez-Mateo and F. Santoyo-Gonzalez, *Bioconjugate chemistry*, 2016, **27**, 549-561.
39. W. Godbey, K. K. Wu and A. G. Mikos, *Journal of biomedical materials research*, 1999, **45**, 268-275.
40. M. Rezaee, R. K. Oskuee, H. Nassirli and B. Malaekeh-Nikouei, *J Control Release*, 2016, **236**, 1-14.
41. W. Chen, W. Deng and E. M. Goldys, *Molecular Therapy-Nucleic Acids*, 2017, **7**, 366-377.
42. A. Høgset, B. Ø. Engesæter, L. Prasmickaite, K. Berg, Ø. Fodstad and G. M. Mælandsmo, *Cancer Gene Ther*, 2002, **9**, 365-371.
43. Z. Li, P. Agharkar and B. Chen, *Cancer Lett*, 2013, **339**, 128-134.
44. A. Elhissi, M. O'Neill, S. Roberts and K. Taylor, *Int J Pharm*, 2006, **320**, 124-130.
45. A. Ewe and A. Aigner, *Non-Viral Gene Delivery Vectors: Methods and Protocols*, 2016, 187-200.
46. M. Diehn, R. W. Cho, N. A. Lobo, T. Kalisky, M. J. Dorie, A. N. Kulp, D. Qian, J. S. Lam, L. E. Ailles and M. Wong, *Nature*, 2009, **458**, 780.
47. K. Purdy, T. Embley, S. Takii and D. Nedwell, *Appl Environ Microb*, 1996, **62**, 3905-3907.
48. A. Kunwar, A. Barik, R. Pandey and K. I. Priyadarsini, *Biochimica et Biophysica Acta (BBA)-General Subjects*, 2006, **1760**, 1513-1520.
49. L. P. T. H. J. Liang, T. W. Chung and Y. Y. H. D. Z. Liu, *Journal of medical and biological Engineering*, 2007, **27**, 29-34.
50. M. Instruments, *MAN0317*, 2004, **1**.
51. D. Needham and R. S. Nunn, *Biophys J*, 1990, **58**, 997-1009.
52. D.-Z. Liu, W.-Y. Chen, L.-M. Tasi and S.-P. Yang, *Colloids and Surfaces A: Physicochemical and Engineering Aspects*, 2000, **172**, 57-67.
53. F. de Meyer and B. Smit, *Proceedings of the National Academy of Sciences*, 2009, **106**, 3654-3658.
54. W. Liu, Y. Wu, C. Wang, H. C. Li, T. Wang, C. Y. Liao, L. Cui, Q. F. Zhou, B. Yan and G. B. Jiang, *Nanotoxicology*, 2010, **4**, 319-330.
55. S. Bolte and F. Cordelieres, *Journal of microscopy*, 2006, **224**, 213-232.
56. H. Kim and W. J. Kim, *Small*, 2014, **10**, 117-126.
57. M. Matsumoto, R. Kishikawa, T. Kurosaki, H. Nakagawa, N. Ichikawa, T. Hamamoto, H. To, T. Kitahara and H. Sasaki, *International journal of pharmaceutics*, 2008, **363**, 58-65.
58. U. Schmidt-Erfurth and T. Hasan, *Survey of Ophthalmology*, 2000, **45**, 195-214.
59. M. Azab, D. S. Boyer, N. M. Bressler, S. B. Bressler, I. Cihelkova, Y. Hao, I. Immonen, J. I. Lim, U. Menchini and J. Naor, *Archives of Ophthalmology*, 2005, **123**, 448.

60. P. Agostinis, K. Berg, K. A. Cengel, T. H. Foster, A. W. Girotti, S. O. Gollnick, S. M. Hahn, M. R. Hamblin, A. Juzeniene and D. Kessel, *Photodynamic therapy of cancer: an update*, World Health Organization, 2011.

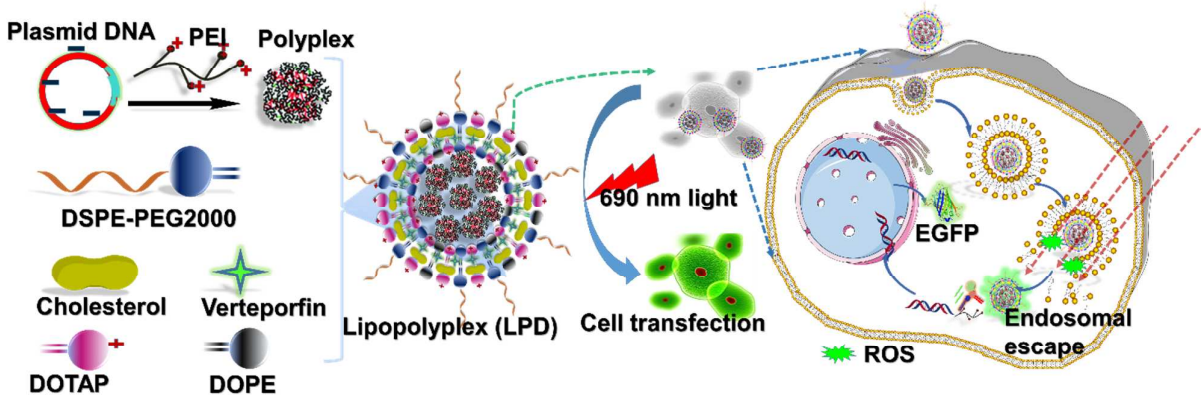

Graphical Table of Contents

Light-triggered endolysosomal escape enhances gene delivery by photoresponsive LPD nanoparticles.

Highlights:

1. Photo responsive lipid-based hybrid nanoparticles were successfully applied for light enhanced the cytoplasmic release of pDNA followed by gene expression

2. Light-triggered endolysosomal escape of pDNA at different time points has been studied at subcellular level, confirming by quantitative analysis of colocalization between pDNA and endolysosomes